Photodetachment cross section of He^- $(1s2s2p\ ^4P^o)$ in the region of the 1*s* detachment threshold

Jinhua Xi
Department of Physics, Vanderbilt University, Nashville, Tennessee 37235

Charlotte Froese Fischer
Department of Computer Science, Vanderbilt University, Nashville, Tennessee 37235

(Received 16 March 1998)

Using a Spline-Garlekin and inverse iteration method, we studied in detail the photodetachment cross section of the He^- $(1s2s2p\ ^4P^o)$ state in the region of the 1*s* detachment threshold. Details of the cross section from threshold to 44 eV are presented. The effects of core excitation and continuum channel coupling are studied. A very narrow $2s3s4s\ ^4S$ resonance was found at 42.866 00 eV with a width of 0.103 meV. Other resonance structures are also found and analyzed. We studied the $2s2p^2\ ^4P$ resonance state that lies immediately below the 1*s* threshold. The width and position of this state, obtained from this calculation, are 37.669 eV and 9.850 meV, respectively. This result is in good agreement with other theoretical calculations.
[S1050-2947(99)01001-X]

PACS number(s): 32.80.Fb, 32.80.Gc

I. INTRODUCTION

The weakly bound He^- negative ion has attracted considerable interest in recent years. Because of the weak coupling among electrons, theoretical calculations cannot predict the resonance behavior correctly if the correlations are not properly included. The $1s2s2p\ ^4P$ metastable state, with an extra electron bound to the $1s2s\ ^3S$ state of He, can be studied via the photodetachment process. From this study the quartet ^4S, ^4P, and ^4D excited states of He^- can be investigated. The energy of this state was calculated by Bunge and Bunge [1]. They obtained the binding energy to be 77.51 ± 0.04 meV. The accuracy of the binding energy was improved by a recent experimental and theoretical study of Kristensen *et al.* [2]. The reported theoretical value was 77.518 ± 0.011 meV, in agreement with their experimental result of 77.516 ± 0.006 meV. There also have been some theoretical [3–7] and experimental [8–14] studies of the photodetachment cross section and angular distribution of the quartet $1s2s2p\ ^4P^o$ state. The $1s2p^2\ ^4P$ sharp resonance has drawn particular attention among all these studies. This resonance was reported by Hazi and Reed [3] in a theoretical study of the photodetachment cross section of the $1s2s2p\ ^4P^o$ state. Thereafter, theoretical [4–6] and experimental [10–12] investigations have been performed that determined the width and position and the maximum cross section of the resonance with high accuracy. In our first paper on the photodetachment study of He^- [6], we calculated the cross section and angular distribution of the $1s2s2p\ ^4P^o$ state with energy from threshold to 4 eV. We employed an approach that uses a spline basis and multiconfiguration Hartree-Fock (MCHF) orbitals to calculate the interaction matrix and the wave functions of the system. The $1s2p^2\ ^4P$ sharp resonance was investigated in detail and excellent agreement with the experimental data was obtained. We also predicted the $1s3s4s\ ^4S$ Feshbach resonance at 2.959 07 eV with a width of 0.19 meV. This result was verified by a recent experiment measurement of Klinkmüller *et al.* [15], which gives 2.959 255(7) eV and 0.19(3) meV for the position and width, respectively.

In this paper we report the calculation of the cross section of the 1*s* photodetachment from the He^- $(1s2s2p\ ^4P^o)$ state, with photon energy from threshold up to 44 eV. In the recent publication of Kim, Zhou, and Manson [7], the photodetachment from the inner 1*s* electron to certain selected channels was studied using the *R*-matrix method with MCHF orbitals, where the energy covered the whole range from threshold to 100 eV. In their paper, the large correlations are considered but fine correlation effects are ignored, so small resonance structures near threshold did not appear. In our calculation described below, however, we intend to provide a more complete study of the resonance structure and photodetachment property in the threshold region of the 1*s* detachment. We also report the result of the $2s2p^2\ ^4P$ Feshbach resonance. The $2s2p^2\ ^4P$ state was predicted by Chung [16] using the saddle-point variation method. Later the resonance position and width were investigated by Bylicki and Nicolaides [17,18], Chung [19], and Kim, Zhou, and Manson [7]. Recently, Morishita and Lin [20] analyzed the resonance states of the He^- system using the hyperspherical idiabatic potential curves.

II. THEORY AND COMPUTATIONAL APPROACH

We use an interaction matrix inverse iteration approach based on the Galerkin method, using MCHF orbitals for bound orbital functions and splines as basis functions for continuum orbitals. The configuration space consists of bound configurations (perturber states) that incorporate fine and weak correlations, closed-channel configurations that include the major correlation effects near threshold, and open-channel configurations that represent the behavior of the photoelectrons. In our earlier paper [6] we described the interaction matrix and Galerkin approach in detail. Briefly, the

final-state wave function after the photodetachment can be described as

$$\Psi(\gamma LS)=\sum_{i=1}^{M_p} c(i)\phi(\alpha_i LS)+\sum_{i=1}^{M_c} |(\tau_i \bullet |\overline{n_i l_i}\rangle)LS\rangle. \quad (1)$$

The bound states $\phi(\alpha_i LS)$ and the target states $|\tau_i\rangle$ are defined in terms of the fixed orbitals from MCHF calculation optimized on an average effect of the wave functions of the initial state and target states of interest. It is crucial that the target states $|\tau_i\rangle$ are represented by multiconfiguration wave functions with high accuracy; single-configuration targets cannot represent the behaviors of the channel states correctly. Orthogonality is required among all target state wave functions and all configuration state wave functions (including perturber-perturber, perturber-channel, and channel-channel functions). We also require that all channel orbital wave functions be orthogonal to all fixed orbital wave functions. Orthogonality among channel orbital wave functions is not required. The radial part of the unnormalized channel wave function $|\overline{n_i l_i}\rangle$ is expanded in terms of a *B*-spline basis set. The channel states can be bound states if the photoenergy is below its threshold energy.

With the channel orbital wave functions expanded in terms of the *B*-spline basis sets and bound orbitals represented in terms of a set of pregenerated MCHF orbitals, the residual of the system can be calculated. We expect that under a good approximation the residual of the system should be zero, i.e.,

$$(H-E)\Psi(\gamma LS)\approx 0; \quad (2)$$

the Galerkin condition requires that the residual be orthogonal to the solution space for a set of test functions. In the current case, the test functions consist of all perturber state wave functions and the channel state wave functions with the channel orbitals being substituted by the spline basis functions. Applying the Galerkin condition, we get the generalized eigenvalue equation

$$\mathbf{(H-ES)C}=0. \quad (3)$$

The inverse iteration method is used to solve the above equation for the continuum orbital wave functions and the weight coefficients of the perturbers for each given energy value. A detailed description of the spline-Galerkin method and the inverse iteration algorithm for continuum state problem can be found in earlier publications [21,22]. A multiple open channel solution was also described in detail in Ref. [6].

The photodetachment cross section (in a.u.) is defined as

$$\sigma=4\pi^2\alpha E|\langle\Psi_E|T|\Psi_0\rangle|^2, \quad (4)$$

where α is the fine-structure constant, E is the photon energy, and Ψ_0 and Ψ_E are the initial and final state wave functions, respectively, represented in terms of the multiconfiguration and/or multichannel states under LS coupling. T is the transition operator. For electric dipole transitions, the operators in length form and velocity form are (in a.u.)

$$T_L^1=\sum_j \vec{r}_j, \quad T_V^1=\sum_j \frac{\vec{\nabla}_j}{iE}. \quad (5)$$

When a resonance appears, its position E_r and width Γ can be determined from the cross section. For a Feshbach resonance, it is determined by fitting the total photodetachment cross section $\sigma(E)$ to the Fano-Cooper formula [23]

$$\sigma(E)=\sigma_0[1+a(E-E_r)]\left[1-\rho^2+\rho^2\frac{(q+\epsilon)^2}{1+\epsilon^2}\right], \quad (6)$$

with

$$\epsilon=2(E-E_r)/\Gamma, \quad (7)$$

where a linear background $\sigma_0[1+a(E-E_r)]$ is assumed in the resonance region. σ_0 is the background cross section at E_r and a is a parameter.

III. RESULTS AND DISCUSSION

A. Bound-state orbital set and final-state configurations

The accuracy of the bound orbitals plays a fundamental role in the accuracy of the current calculation. Unlike the channel orbitals that are determined dynamically via the channel coupling, the bound orbitals are fixed throughout the process in determining the final state wave function. Because of this, we need to generate these orbitals with the highest possible accuracy. Since we use the same orbital set to generate the initial state wave function, the final perturber state wave function, and the target state wave function, we need a special optimization algorithm to produce the best average result. The orbitals are generated as follows. Orbitals with $n\leqslant 5$ are taken from the orbital set of Ref. [6]; other orbitals are optimized so that best average results can be obtained for the initial state and target states of interest. Specifically, orbitals with $n=6,7,8$ are optimized for the $2s2p\ ^3P$ state and orbitals with $n=9,10$ are optimized for initial state. The initial state energy obtained here is -2.1780499 a.u. The orbitals with $n<10$ are used to generate target state configurations and final state bound perturbers. Orbitals with $n=10$ are included in the configuration set of the initial state wave function. The energies of target states are shown in Table I.

The final state configurations are formed by coupling the target states in Table I with appropriate channel orbitals. Since the inner-shell excitations are involved for photoenergy higher than 38.5 eV, the size of the channel set might be very large. It is very important in the current approach to include all possible channels unless the corresponding component of the bound perturbers for any missing channel also is removed from the configuration list of the final states since these components may produce a pseudoresonance if the channel components are not included. In our calculation described below, we include $1s2s\ ^3S$, $1s3s\ ^3S$, $1s2p\ ^3P^o$, $1s3p\ ^3P^o$, and $1s3d\ ^3D$ from the lowest target states and all target states above the $1s$ threshold and up to 44 eV, which include all targets with inner $2s$ and $2p$ orbitals. These target states are then coupled with possible channel orbitals to form the channel states. All possible channels for the final states within the energy of interest are shown in Table II.

TABLE I. Energies of interested target states and their relative values in eV to the initial state. The energy of the initial state is −2.178 049 9 a.u. (1 a.u.=27.207 613 4 eV is used to convert a.u. to eV.)

Target	Energy (a.u.)	Relative (a.u.)	Relative (eV)
He($1s2s\,^3S$)	−2.175 202 8	0.002 847 1	0.077 46
He($1s2p\,^3P^o$)	−2.133 157 4	0.044 892 5	1.221 42
He($1s3s\,^3S$)	−2.068 683 3	0.109 366 6	2.975 60
He($1s3p\,^3P^o$)	−2.058 058 3	0.119 991 6	3.264 69
He($1s3d\,^3D$)	−2.055 636 2	0.122 413 7	3.330 58
He($2s2p\,^3P^o$)	−0.760 458 6	1.417 591 3	38.569 28
He($2p^2\,^3P$)	−0.710 491 8	1.467 558 1	39.928 75
He($2s3s\,^3S$)	−0.602 486 5	1.575 563 4	42.867 32
He($2s3p\,^3P^o$)	−0.584 580 0	1.593 469 9	43.354 51
He($2p3p\,^3D$)	−0.583 669 0	1.594 380 9	43.379 30
He($2p3s\,^3P^o$)	−0.578 989 8	1.599 060 1	43.506 61
He($2p3p\,^3P$)	−0.567 728 7	1.610 321 2	43.813 00
He($2p3d\,^3F^o$)	−0.565 927 8	1.612 122 1	43.861 99
He($2s3d\,^3D$)	−0.560 198 4	1.617 851 5	44.017 88
He($2p3p\,^3S$)	−0.558 841 0	1.619 208 9	44.054 81
He($2p3d\,^3P^o$)	−0.548 813 1	1.629 236 8	44.327 64
He($2s4s\,^3S$)	−0.548 217 0	1.629 832 9	44.343 86

B. Photodetachment of the 2*s* and 2*p* electrons and the $2s2p^2\,^4P$ resonance

The photodetachment cross section is studied in the energy region of the $2s2p^2\,^4P$ resonance. The $2s2p^2\,^4P$ resonance is found below the $2s2p\,^3P^o$ threshold as a Feshbach resonance. To calculate this resonance state, we include the target states $1s2p\,^3P^o$, $1s3p\,^3P^o$, $1s3d\,^3D$, and $2s2p\,^3P^o$ to construct the channel wave functions. All these target wave functions are multiconfiguration wave functions. For the ^4P final state, the coupled channel states are $1s2pkp\,^4P$, $1s3pkp\,^4P$, $1s3dkd\,^4P$, and $2s2pkp\,^4P$. In Fig. 1 we show the cross section to the final ^4P state in the region of the resonance. The results in length form and in velocity form agree with each other, with a difference of 0.03% at the peak of the resonance. The resonance is dominated by the coupling between the $1s2pkp\,^4P$ channel and the $2s2p^2\,^4P$ perturber state. We fit the total cross section to the Fano-Cooper formula in the energy region between 37.60 eV and 37.75 eV. The position and width of the $2s2p^2\,^4P$ resonance are determined to be 37.669 eV and 9.850 meV, respectively. Both cross sections for the length form and the velocity form fit to the same result. The results obtained here are smaller than but quite close to the most recent results of Chung [19]. Chung used a saddle-point complex-rotation method and calculated the position and width to be 37.670 16 eV and 9.867 meV, respectively. The values reported by

TABLE II. Channel wave functions for the final states. The target energies relative to the initial state are also included. The energy of the initial state is −2.178 049 9 a.u. (1 a.u.=27.207 613 4 eV is used to convert a.u. to eV.)

Target	Energy (eV)	^4P	^4S	^4D
He($1s2s\,^3S$)	0.077 46		ks_1	kd_1
He($1s2p\,^3P^o$)	1.221 42	kp_1	kp_1	kp_1,kf_1
He($1s3s\,^3S$)	2.975 60		ks_2	kd_2
He($1s3p\,^3P^o$)	3.264 69	kp_2	kp_2	kp_2,kf_2
He($1s3d\,^3D$)	3.330 58	kd_1	kd_1	ks_1,kd_3,kg_1
He($2s2p\,^3P^o$)	38.569 28	kp_3	kp_3	kp_3,kf_3
He($2p^2\,^3P$)	39.928 75	ks_1,kd_2		kd_4
He($2s3s\,^3S$)	42.867 32		ks_3	kd_5
He($2s3p\,^3P^o$)	43.354 51	kp_4	kp_4	kp_4,kf_4
He($2p3p\,^3D$)	43.379 30	kd_3	kd_2	ks_2,kd_6,kg_2
He($2p3s\,^3P^o$)	43.506 61	kp_5	kp_5	kp_5,kf_5
He($2p3p\,^3P$)	43.813 00	ks_2,kd_4		kd_7
He($2p3d\,^3F^o$)	43.861 99	kf_1	kf_1	kp_6,kf_6,kh_1
He($2s3d\,^3D$)	44.017 88	kd_5	kd_3	ks_3,kd_8,kg_3
He($2p3p\,^3S$)	44.054 81		ks_4	kd_9
He($2p3d\,^3P^o$)	44.327 64	kp_6	kp_6	kp_7,kf_7

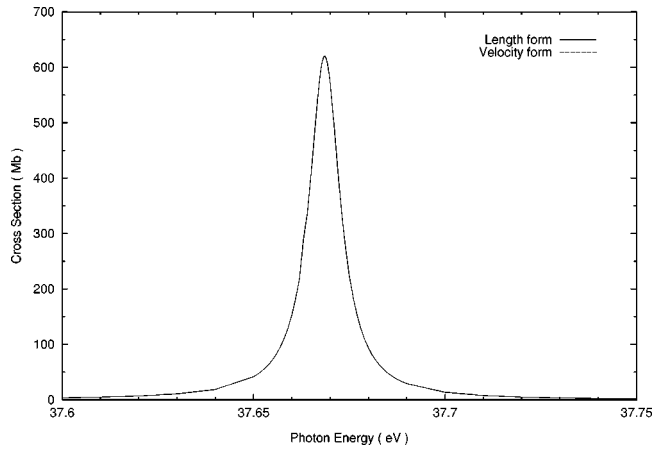

FIG. 1. Partial cross section of the $He^-(1s2s2p\ ^4P^o)$ photodetachment to the final ^4P state showing the $2s2p^2\ ^4P$ resonance. We can see that the cross section for the length form and velocity form agree very well, with a difference of 0.03% at the peak of the resonance.

Kim, Zhou, and Manson [7] are 37.683 eV and 9.22 meV for the position and width, respectively. Bylicki and Nicolaides [17,18] investigated this resonance using a complex-coordinate rotation method; the results they obtained are 37.672 eV and 10.3 meV, respectively. A detail comparison of the width and position of this resonance is given in Table III. We need to mention here that the $2s2p^2\ ^4P$ resonance has an unsymmetric shape that is not obvious from Fig. 1. We can see later from Table IV that this resonance has a very large negative q value.

C. Photodetachment of the 1s electron

A detailed calculation in the threshold region of the 1s electron detachment is performed. The photon energy covers the region from 38.5 eV to 44 eV. The target states above the 1s detachment threshold are $(2s2p,2s3p,2p3s)\ ^3P^o$, $2p^2\ ^3P$, $2s3s\ ^3S$, and $2p3p\ ^3P,^3D$. Except for the lowest $2s2p\ ^3P^o$ target state, photodetachment via other target states represents the detachment plus target excitations. Among the $^3P^o$ target states, the energy positions of the $2s3p\ ^3P^o$ and $2p3s\ ^3P^o$ states are very close with each other. Channels from these target states may have a strong correlation effect that can be found from their photodetachment cross sections.

TABLE III. Position and width of the $2s2p^2\,^4P$ resonance compared with those from other theoretical calculations.

Reference	Position (eV)	Width (meV)
[19]	37.670 16	9.867
[7]	37.683	9.22
[17,18]	37.672	10.3
this work	37.669	9.850

The photodetachment cross section for the ^4P final state is shown in Fig. 2. The cross section for the $2s2p(^3P^o)kp\ ^4P$ channel has a smooth increase from its threshold and reaches a maximum of 3.4 Mb at 39.05 eV. There is a sharp peak at 40.02 eV and a very small rise after the peak at 40.3 eV. These are the contributions of the $2p^2(^3P)ks\ ^4P$ and $2p^2(^3P)kd\ ^4P$ channels. Though the absolute values of the cross section at these peaks are not large, the partial cross section of each channel shows that there is a strong channel-channel interaction between these two channels in the energy region of the second and third peaks. We should mention that for these two channels, the process is not simply the 1s detachment plus core excitation. It involves the excitation of the two electrons in the s orbitals into the p orbital and the detachment of one of the p electrons. To explain this, we should keep in mind that our initial state is expanded in terms of multiconfiguration wave functions. So the $1s2s2p\ ^4P^o$ state contains excited configurations such as $2p^3\ ^4P^o$ as components.

The large resonance at 43.353 eV is caused mainly by the $2s3p^2\ ^4P$ perturber state. This resonance appears at the energy region where the $2s3p\ ^3P^o$ state is located. There are also some small peaks at an energy above 43.5 eV. These peaks are the contributions of the $(2s3p,2p3s)kp\ ^4P$ channels. In Fig. 3 we show the partial cross sections of the $2s3p(^3P^o)kp\ ^4P$ and the $2p3s(^3P^o)kp\ ^4P$ channels. We can see that a strong interaction exists at around 43.75 eV when both channels are open.

In Fig. 4 we show the cross section to the final ^4S state. The most interesting part in this figure is the narrow reso-

TABLE IV. Resonance position (E_r) and width (Γ) and other parameters (σ_0, a, ρ, and q) from the Fano-Cooper formula [Eqs. (6) and (7)] for the resonance states identified in this paper. The energy ranges (eV) of the resonances are also listed. The parameters are determined by fitting the Fano-Cooper formula to the cross section for both the length form and the velocity form in the defined energy ranges.

Parameter	$2s2p^2\,^4P$		$2s3p^2\,^4P$		$2s3s4s\,^4S$		$2p3s(^3P^o)3p\,^4D$	
	Length	Velocity	Length	Velocity	Length	Velocity	Length	Velocity
Range (eV)	37.60–37.75		43.2–43.5		42.865–42.867		43.25–43.65	
σ_0 (Mb)	0.3	0.3	0.410	0.416	0.494	0.450	0.2	0.2
a	0.018 6	0.018 6	−0.176	−0.162	−0.547	−0.593	0.1	0.1
ρ	−0.260	−0.260	−0.824	−0.810	−0.818	−0.827	−0.001 1	−0.001 2
q [a]	−174.64	−174.64	−14.52	−14.41	−12.29	−8.08	−12880.7	−11907.1
E_r (eV)	37.669	37.669	43.353	43.353	42.866 00	42.866 00	43.486	43.486
Γ (meV)	9.850	9.850	12.607	12.589	0.103	0.102	23.009	23.016

[a]When $\rho\to 0$, $q\to\infty$, but $q'=q\rho$ is a limited value. So q' is used in the fitting process.

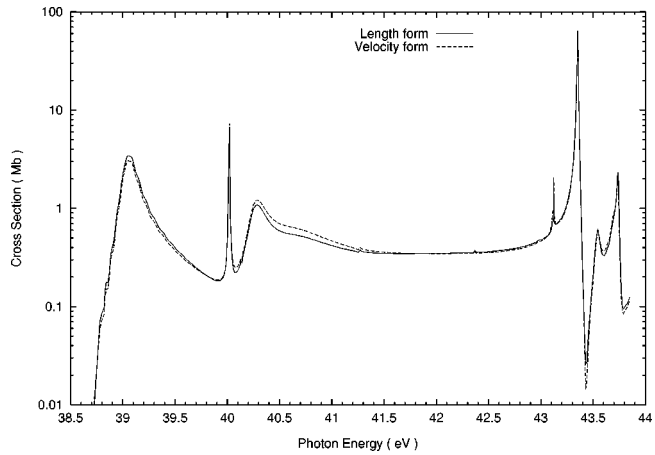

FIG. 2. Partial $1s$ detachment cross section of the $He^-(1s2s2p\ ^4P^o)$ photodetachment to the final ^4P states. The first peak of the cross section is contributed by the $2s2p(^3P^o)kp\ ^4P$ channel. The peaks at 40 eV and 40.3 eV are caused by the $2p^2(^3P)ks\ ^4P$ and $2p^2(^3P)kd\ ^4P$ channels. The large peak at 43.352 eV indicates the $2s3p^2\ ^4P$ resonance. The peaks after this resonance show the interaction between the $2s3p(^3P^o)kp\ ^4P$ and the $2p3s(^3P^o)kp\ ^4P$ channels.

nance at 42.866 00 eV, with a width of 0.103 meV. This resonance is located 1.3 meV below the energy of the $2s3s\ ^4S$ target state and is identified as the $2s3s4s\ ^4S$ resonance state. It is interesting to compare this resonance with the $1s3s4s\ ^4S$ resonance predicted in our earlier paper [6] and verified experimentally by Klinkmüller *et al.* [15]. The $1s3s4s\ ^4S$ resonance was located 17 meV below the $1s3s\ ^3S$ state of He, with a width of 0.19 meV. Both resonances have a very small width and thus have very small interaction with the continuum channels. The cross sections from the length form and velocity form in the region of the $2s3s4s\ ^4S$ resonance do not agree with each other. The cross section at the peak of the resonance is 50.3 Mb for the length form, but only 20.5 Mb for the velocity form. This discrepancy is caused by the incompleteness of the bound perturber configuration set. By studying the weight coefficients of the bound perturber states and closed channel states, we found that the $2s3sks\ ^4S$ closed channel plays an important rule in the cross section; this indicates indirectly that more correlation among bound perturbers and bound channels needs to be included. Since the bound orbitals are optimized based on the low energy states, a resonance such as the $1s3s4s\ ^4S$ state can be predicted with high accuracy. However, the $2s3s4s\ ^4S$ state lies at a position much higher than that of the $1s3s4s\ ^4S$ state. The fixed orbitals used here are not good enough to predict accurately such narrow resonances at such high energy. We also verified the behavior of the channel orbital wave functions at the resonance region; we found that both the open channel orbital (the kp orbital for $2s2pkp\ ^4S$) wave function and the closed channel orbital (the ns orbital for the $2s3sns\ ^4S$) wave function have the correct behavior. The wave function of the ns orbital converges very well within the cutoff radius of 500 a.u. Though the values of the cross sections for the length form and velocity form do not agree in the region of this resonance, the values of the position and width agree very well.

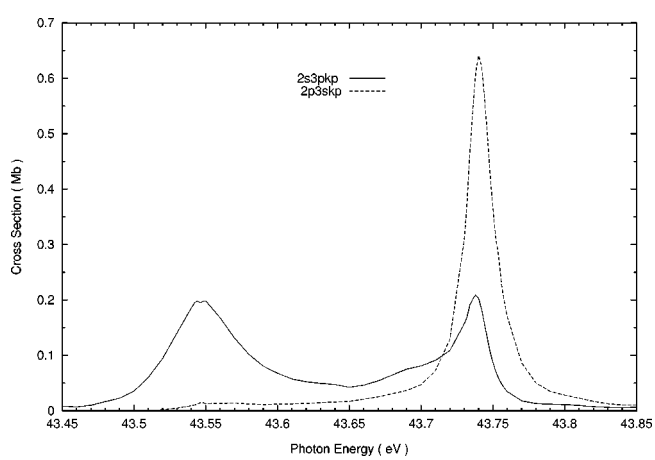

FIG. 3. Partial cross sections from the $2s3p(^3P^o)kp\ ^4P$ and the $2p3s(^3P^o)kp\ ^4P$ channels. The strong interaction between these two channels is shown at energy near 43.75 eV.

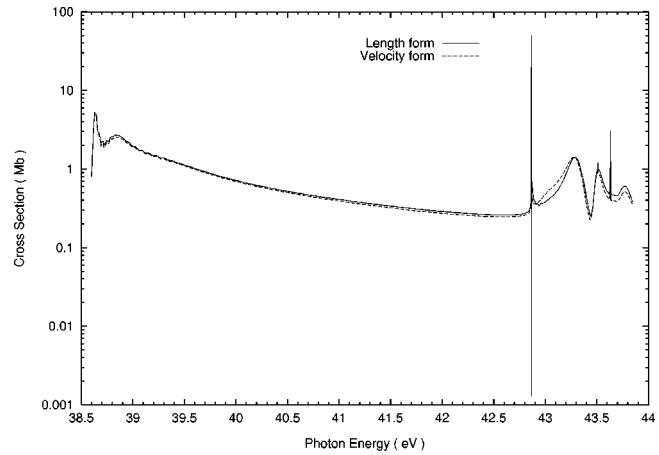

FIG. 4. Contribution of the partial $1s$ detachment cross section from the final ^4S state. From this figure we can see the narrow $2s3s4s\ ^4S$ resonance.

The photodetachment cross sections for the final ^4D state are shown in Fig. 5. The first two peaks are the result of the

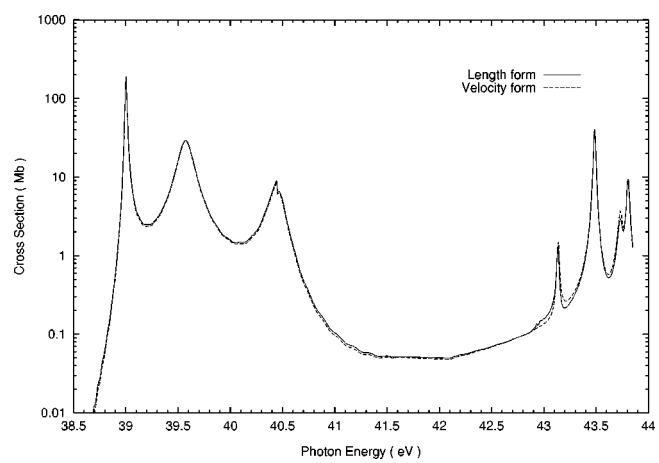

FIG. 5. Partial $1s$ detachment cross section to the final ^4D state. The first two peaks in the figure are caused by the interaction of the $2s2p(^3P^o)kp\ ^4D$ channel and the $2s2p(^3P^o)kf\ ^4D$ channel. The third peak is from the $2p^2(^3P)kd\ ^4D$ channel. The peak at 43.486 eV is a resonance caused by the $2p3s(^3P^o)3p\ ^4D$ perturber state.

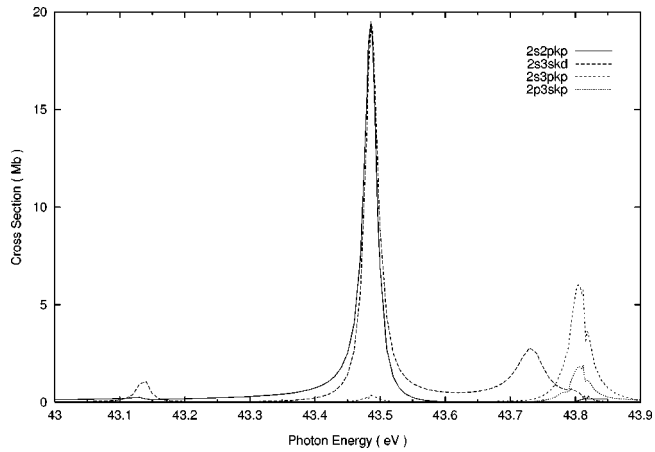

FIG. 6. Partial cross sections from the $2s2pkp\ ^4D$, $2s3skd\ ^4D$, $2s3pkp\ ^4D$, and $2p3skp\ ^4D$ channels. Only the result from the length form is plotted in the figure. The difference between the velocity form and the length form at the peak of each partial cross section is 5% for the $2s2pkp\ ^4D$ channel and the $2s3skd\ ^4D$ channel and 9% for the $2s3pkp\ ^4D$ channel and the $2p3skp\ ^4D$ channel. The first peak at 43.135 eV is from the $2s3s(^3S)kd\ ^4D$ channel. The large resonance at 43.486 eV is caused by the $2p3s(^3P^o)3p\ ^4D$ perturber state. The cross sections for both the $2s2pkp\ ^4D$ channel and the $2s3skd\ ^4D$ channel have a maximum value of about 20 Mb at the resonance position. The peak at 43.81 eV shows the channel interaction between the $2s3pkp\ ^4D$ channel and the $2p3skp\ ^4D$ channel when the cross section from the $2p3skp\ ^4D$ channel reaches its maximum.

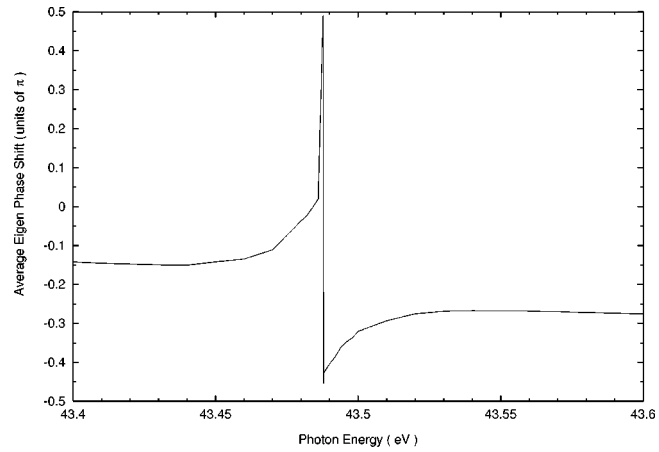

FIG. 7. Average eigenphase shift for the $2s2pkp\ ^4D$ channel and the $2s3skd\ ^4D$ channel at the resonance region of the $2p3s(^3P^o)3p\ ^4D$ perturber state. We can see from the figure that the average eigenphase shift has a change of π at 43.486 eV.

$2s2p(^3P^o)(kp,kf)\ ^4D$ channels. The cross section for the $2s2p(^3P^o)kp\ ^4D$ channel has a rapid increase in the threshold to a maximum of about 200 Mb, followed by a deep decrease. Since the $2s2p(^3P^o)kf\ ^4D$ channel is also open, the coupling of these two channels causes the cross section from the final ^4D state to increase after the first peak and reach the second maximum at 39.6 eV as shown in Fig. 5. The third peak in Fig. 5 is from the $2p^2(^3P)kd\ ^4D$ channel. Compared to Fig. 2, we can see that the $2p^2(^3P)kd\ ^4D$ channel makes a much larger contribution than the $2p^2(^3P)kd\ ^4P$ channel does to the cross section. Again, similar to the $2p^2(^3P)(ks,kd)\ ^4P$ channels, the $2p^2(^3P)kd\ ^4D$ channel represents photodetachment plus core excitation from multiconfiguration initial states. Figure 5 also shows a peak of about 40 Mb at 43.486 eV. This peak is contributed from the cross section of the $2s2p(^3P^o)kp\ ^4D$ channel and the $2s3s(^3S)kd\ ^4D$ channel. According to the value of the weight coefficients for the perturber states, this maximum is mainly caused by the $2p3s(^3P^o)3p\ ^4D$ perturber state. Since there are several channels open at this energy region, this peak may also be considered as the result of the interaction of these open channels. To clarify this, we plot in Fig. 6 the partial cross sections of the open channels in this region: the $2s2pkp\ ^4D$ channel with a threshold at 38.569 28 eV, the $2s3skd\ ^4D$ channel with a threshold at 42.867 32 eV, the $2s3pkp\ ^4D$ channel with a threshold at 43.354 51 eV, and the $2p3skp\ ^4D$ channel with a threshold at 43.506 61 eV. Only the result from the length form is plotted in the figure. The difference between the velocity form and the length form at the peak of each partial cross section is 5% for the $2s2pkp\ ^4D$ channel and the $2s3skd\ ^4D$ channel and 9% for the $2s3pkp\ ^4D$ channel and the $2p3skp\ ^4D$ channel. The $2p^2(^3P)kd\ ^4D$ channel has little contribution to the cross section and will not be considered here. First, we look at the peak in Fig. 6 at 43.135 eV. This peak is caused by the cross section of the $2s3s(^3S)kd\ ^4D$ channel and has little effect on the cross section of the $2s2pkp\ ^4D$ channel, indicating that the interaction between these two channels is negligible. Because of this, the large resonance at 43.486 eV cannot be the result of a channel interaction from these two channels. Next we see that the cross section of the $2s3pkp\ ^4D$ channel has only a small rise at the position of the large peak. When the channel couples with the $2p3skp\ ^4D$ channel, however, it causes a significant rise for the cross sections of both channels at about 43.81 eV. Unlike the $2s3pkp\ ^4D$ and $2p3skp\ ^4D$ channels, whose target energies are very close to each other (and thus a strong channel interaction is expected), the $2s2pkp\ ^4D$ channel and the $2s3pkp\ ^4D$ channel should have a much smaller channel interaction because the energies of the target states differ considerably. It is indeed the case as we can see from Fig. 6 since the first rise for the cross section of the $2s3pkp\ ^4D$ channel is very small, whereas the second rise is much larger. So we conclude that the peak at 43.486 eV from the cross section of the $2s2pkp\ ^4D$ channel and the $2s3skd\ ^4D$ channel is a resonance due to the interaction of these channels with the $2p3s(^3P^o)3p\ ^4D$ perturber and other perturber configurations from the $2p3s\ ^3P^o$ target state. This conclusion is also supported by the average eigenphase shift shown in Fig. 7, which shows a change of π at an energy around 43.486 eV, indicating a resonance in this region.

The total $1s$ detachment cross section is shown in Fig. 8. There is a large, steep rise from the threshold to a maximum of about 200 Mb at 39.002 eV followed by a deep decrease. This is the photodetachment cross section via the $2s2p(^3P^o)kp(^4P,^4D)$ channels. This result is similar to the result of Kim, Zhou, and Manson [7], who also find a rapid rise at the threshold but with a much slower decrease after the maximum. The maximum value in their calculation is about 30 Mb, much smaller than our result of 200 Mb. From Fig. 5 we can see that this peak is dominated by the partial

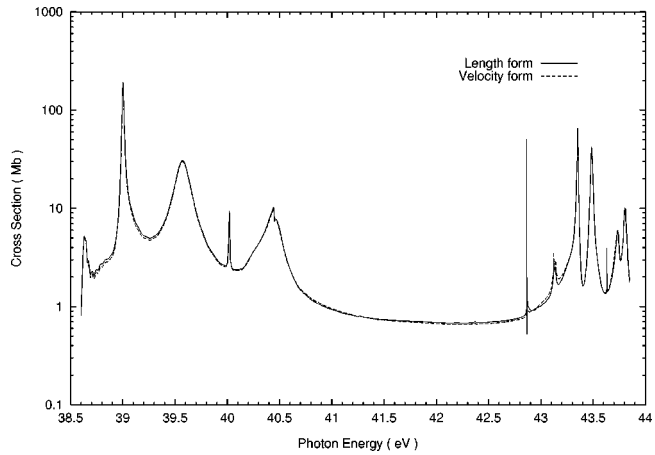

FIG. 8. Total cross section from the $1s$ detachment channels. The large peak at 39 eV is mainly from the $2s2pkp\ ^4D$ detachment channel. Below 43 eV we can see the $2s3s4s\ ^4S$ resonance. Detailed structures are also shown at an energy around 43.5 eV, including the $2s3p^2\ ^4P$ and the $2p3s(^3P^o)3p\ ^4D$ resonances.

cross section for detachment to the final ^4D state.

Finally, we summarize in Table IV the resonance states found in this investigation. There are four resonance states in the energy region covered in this paper: the $2s2p^2\ ^4P$ state at 37.669 eV with a width of 9.850 meV, the $2s3p^2\ ^4P$ state at 43.353 eV with a width of 12.60 meV, the $2s3s4s\ ^4S$ state at 42.866 00 eV with a width of 0.103 meV, and the $2p3s(^3P^o)3p\ ^4D$ state at 43.486 eV with a width of 23.01 meV.

D. Total cross sections

In Fig. 9 we show the total photodetachment cross section from the He$^-$ $(1s2s2p\ ^4P^o)$ initial state. Data with energies below 4 eV are taken from Ref. [6]. The theoretical results of Kim, Zhou, and Manson are also shown in the figure. We can see that the two theoretical results agree reasonably well, particularly in the area of the $1s2p^2\ ^4P$ and $2s2p^2\ ^4P$ resonances. Both calculations show an asymmetric shape for the $2s2p^2\ ^4P$ resonance. The asymmetric shape is more obvious in the result of Kim, Zhou, and Manson since their cross section keeps decreasing after the peak of the $2s2p^2\ ^4P$ resonance until the energy reaches the threshold energy of the He$(2s2p\ ^3P^o)$ target state. In our calculation, however, the cross section reaches the minimum value and begins to increase before the energy reaches that of the

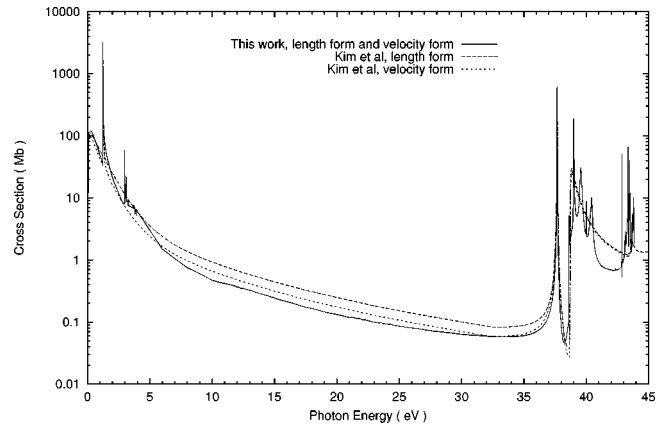

FIG. 9. Total cross section from the He$^-$ $(1s2s2p\ ^4P^o)$ initial state. The results of Kim, Zhou, and Manson are also shown in the figure.

He $(2s2p\ ^3P^o)$ target state. This difference can be interpreted as the result of channel coupling between the open channels and the $2s2p(^3P^o)np\ ^4P$ closed channel. In the energy region above 40 eV, the result of Kim, Zhou, and Manson does not give the detailed resonance structures shown in our calculation. This is expected since the small correlation effects are ignored in their calculation.

IV. CONCLUSION

We studied in detail the photodetachment cross sections of the $1s2s2p\ ^4P^o$ state of the He$^-$ negative ion in the region of the $1s$ detachment threshold. Detachment of both the inner $1s$ electron and the outer $2s,2p$ electrons is investigated. The calculation for the $2s2p^2\ ^4P$ Feshbach resonance is in good agreement with other theoretical results. We exploited the photodetachment of the inner $1s$ electron in the threshold region and observed detailed resonance structures. In particular we identified a very narrow $2s3s4s\ ^4S$ Feshbach resonance. This resonance is quite similar to the $1s3s4s\ ^4S$ resonance we found in an earlier calculation.

ACKNOWLEDGMENTS

Thanks are due to Dr. Hsaio-Ling Zhou for sending us the numerical data of their calculation. This research was supported by the Division of Chemical Sciences, Office of Basic Energy Sciences, Office of Energy Research, U.S. Department of Energy.

[1] A.V. Bunge and C.F. Bunge, Phys. Rev. A **30**, 2179 (1984).
[2] P. Kristensen, U.V. Pedersen, V.V. Petrunin, T. Andersen, and K.T. Chung, Phys. Rev. A **55**, 978 (1997).
[3] A.U. Hazi and K. Reed, Phys. Rev. A **24**, 2269 (1981).
[4] L.V. Chernysheva, G.F. Gribakin, V.K. Ivanov, and M.Vu. Kuchiev, J. Phys. B **21**, L419 (1988).
[5] H.P. Saha and R.N. Compton, Phys. Rev. Lett. **64**, 1510 (1990).
[6] Jinhua Xi and Charlotte Froese Fischer, Phys. Rev. A **53**, 3169 (1996).
[7] D.S. Kim, H.L. Zhou, and S.T. Manson, Phys. Rev. A **55**, 414 (1997).
[8] R.N. Compton, G.D. Alton, and D.J. Pegg, J. Phys. B **13**, L651 (1980).
[9] R.V. Hodges, M.J. Coggiola, and J.R. Peterson, Phys. Rev. A **23**, 59 (1981).
[10] J.R. Peterson, M.J. Coggiola, and Y.K. Bae, Phys. Rev. Lett. **50**, 664 (1983).
[11] J.R. Peterson, Y.K. Bae, and D.L. Huestis, Phys. Rev. Lett. **55**, 692 (1985).

[12] C.W. Walter, J.A. Seifert, and J.R. Peterson, Phys. Rev. A **50**, 2257 (1994).
[13] D.J. Pegg, J.S. Thompson, J. Dellwo, R.N. Compton, and G.D. Alton, Phys. Rev. Lett. **64**, 278 (1990).
[14] J.S. Thompson, D.J. Pegg, R.N. Compton, and G.D. Alton, J. Phys. B **23**, L15 (1990).
[15] A.E. Klinkmüller, G. Haeffler, D. Hanstorp, I.Y. Kiyan, U. Berzinsh, C.W. Ingram, D.J. Pegg, and J.R. Peterson, Phys. Rev. A **56**, 2788 (1997).
[16] K.T. Chung, Phys. Rev. A **20**, 724 (1979).
[17] M. Bylicki and C.A. Nicolaides, Phys. Rev. A **48**, 3589 (1993).
[18] M. Bylicki and C.A. Nicolaides, Phys. Rev. A **51**, 204 (1995).
[19] Kwong T. Chung, Phys. Rev. A **51**, 844 (1995).
[20] T. Morishita and C.D. Lin, J. Phys. B **31**, L209 (1998).
[21] C. Froese Fischer and M. Idrees, Comput. Phys. **3**, 53 (1989).
[22] T. Brage, C. Froese Fischer, and G. Miecznik, J. Phys. B **25**, 5298 (1992), and references cited therein.
[23] U. Fano and J.W. Cooper, Phys. Rev. **137**, A1364 (1965).